

Розглянуто новий двоканальний ємнісний МЕМС гравіметр автоматизованої авіаційної гравіметричної системи, точність якого вище відомих сьогодні гравіметрів. Описано його конструкцію та проведено моделювання підвісу складної форми. Досліджено за допомогою ЕОМ вплив частот та амплітуд збурюючих дій для найнесприятливіших резонансних випадків двоканального ємнісного гравіметра. Доведено можливість та доцільність використання у якості гравіметра АГС двоканального ємнісного МЕМС гравіметра

Ключові слова: двоканальний ємнісний гравіметр, МЕМС гравіметр, авіаційна гравіметрична система, прискорення сили тяжіння, чутливий елемент

Рассмотрен новый двухканальный емкостной МЭМС гравиметр автоматизированной авиационной гравиметрической системы, точность которого выше известных сегодня гравиметров. Описана его конструкция и проведено моделирование подвеса сложной формы. Исследованы с помощью ЭВМ влияние частот и амплитуд возмущающих воздействий для самых неблагоприятных резонансных случаев двухканального емкостного гравиметра. Доказано возможность и целесообразность использования в качестве гравиметра АГС двухканального емкостного МЭМС гравиметра

Ключевые слова: двухканальный емкостной гравиметр, МЭМС гравиметр, авиационная гравиметрическая система, ускорение силы тяжести, чувствительный элемент

UDC 528.563

DOI: 10.15587/1729-4061.2016.85463

SIMULATION OF INFLUENCE OF PERTURBATION PARAMETERS ON THE NEW DUAL-CHANNEL CAPACITIVE MEMS GRAVIMETER PERFORMANCE

O. Bezvesilna

Doctor of Technical Sciences, Professor,
Honored Worker of Science of Ukraine*

E-mail: bezvesilna@mail.ru

T. Khylichenko

Postgraduate Student**

E-mail: xvulunka@mail.ru

A. Tkachuk

PhD**

E-mail: andrew_tkachuk@i.ua

S. Nechai

PhD, Associate Professor*

*Department of Instrumentation

National Technical University of Ukraine

«Igor Sikorsky Kyiv Polytechnic Institute»

Peremohy ave., 37, Kyiv, Ukraine, 03057

**Department of automation and computer-integrated technologies named after prof. B. B Samotokin

Zhytomyr State Technological University

Chernyakhovskogo str., 103, Zhytomyr, Ukraine, 10005

1. Introduction

At present, it is very important to use the aviation gravimetric system (AGS) for the exploration of minerals (geology, geophysics, geodesy), for the correction of inertial navigation systems (aerospace technology) for the location of moving objects in the water areas of seas and oceans, for the realizations of tasks in archaeology, prediction of earthquakes, etc. Gravimetric measurements are carried out at the surface of the Earth, in submarines, surface ships and aircrafts (AC). Measurements at AC make it possible to receive information about the acceleration of gravity (AG) in remote areas of the globe at velocity much larger than that on the surface.

Traditional air sea gravimetry differs by somewhat outdated technology and inadequate levels of accuracy. And it is characterized by low productivity, minuteness, efficiency, high material costs [1]. At the same time, solving the problem is possible through the use of an onboard miniature navigation complex based on microelectromechanical systems and technologies (MEMS) that combine microelectronic and micromechanical components [2, 3].

At present there are no [1, 4] scientific-theoretical and practical papers that address research into the possibility and expediency of using dual-channel capacitive MEMS gravimeter as an AGS gravimeter. Therefore, it is advisable to explore gravimeters of this type, since they have significant advantages (cancellation of vertical acceleration, instrumental and other errors [5]).

2. Literature review and problem statement

Capacitive gravimeter (CG) measures the acceleration both in the positive and negative direction. CG can measure static accelerations and vibrations with high precision. The main part of gravimeter is a symmetrical sensing element (SE), made by the technology of volumetric micromechanics, which has two sensing capacitors [4]. This decreases dependence on temperature and sensitivity to cross accelerations and increases linearity.

Almost all of the known gravimeters measure the error of vertical acceleration [6], which exceeds the useful signal by dozens of times. They need a long periodic calibration and

setting [7], which significantly complicates the work. Existing innovations deal with the sub-, surface- [8, 9] and terrestrial [10] measurement methods that are not applicable in the aviation gravimetry.

One of the most promising of the known gravimeters at present is a capacitive single-channel gravimeter. It is the primary sensing element of the designed automated AGS [11]. Parameters of the sensing element of CG are selected so that the frequency of its own oscillations equals the highest frequency of gravitational accelerations, which can be measured against the background perturbations. In other words, the sensing element of gravimeter performs the functions of low-pass filter as well. This eliminates the impact on CG initial indications of the errors whose frequency is higher than the frequency of the CG own oscillations, and it increases the accuracy of measuring the acceleration of gravity. However, the single-channel CG does not imply the elimination of errors caused by the influence of vertical acceleration and instrumental errors.

Over the last 20 years, only quartz, strongly damped, gravimeters have been used as the aviation gravimeters, as well as string gravimeters, gyroscopic gravimeters [4]. No measurements have been performed with capacitive gravimeters measurement at all, probably because capacitive transducers only in recent years have been widely applied in various sectors of instrument making. Capacitive transducers, which laid the basis for the capacitive gravimeter, have significant advantages over other converters: high sensitivity and accuracy, small size and weight. The development of MEMS technologies has opened up new opportunities for faster, cheaper and technologically efficient fabrication of capacitive gravimeters that used to be inaccessible.

The accuracy of currently existing gravimeters is insufficient, only (1–5) mGal [4]. Most of them are non-automated. Measurement results' processing is conducted after the AC flight, it is ground-based and takes months to complete. In addition, these gravimeters measure, along with the acceleration of gravity, vertical acceleration of AC \ddot{h} , which is a complicated scientific and technical issue and requires the use of additional filters. There are no studies on the possibility and expediency of using, as the gravimeter, the dual-channel capacitive MEMS gravimeter, which is more accurate (0.5 mGal compared to 1 mGal) that the closest analogue [11].

3. The purpose and objectives of the study

The purpose of this work is to substantiate the possibility of using the dual-channel capacitive MEMS gravimeter as an AGS gravimeter.

To achieve the formulated purpose, the following tasks were set:

- to simulate the impact of load on the suspension of a capacitive MEMS gravimeter;
- to explore the work of the new gravimeter in the most unfavorable resonance cases.

4. Research into stability and the simulation of influence of perturbing action on a dual-channel capacitive MEMS gravimeter

4.1. Design of dual-channel capacitive gravimeter

A modification of the standard design (that comprises an immobile base connected to the body and a frame with the

sensing element, fixed to the upper movable plate) is the oppositely-pin arrangement of electrodes of the plate (Fig. 1): the movable electrodes are placed on the inertial mass, which is attached to the crystal using elastic suspensions. The immovable electrodes are located to the right and to the left of the movable electrodes.

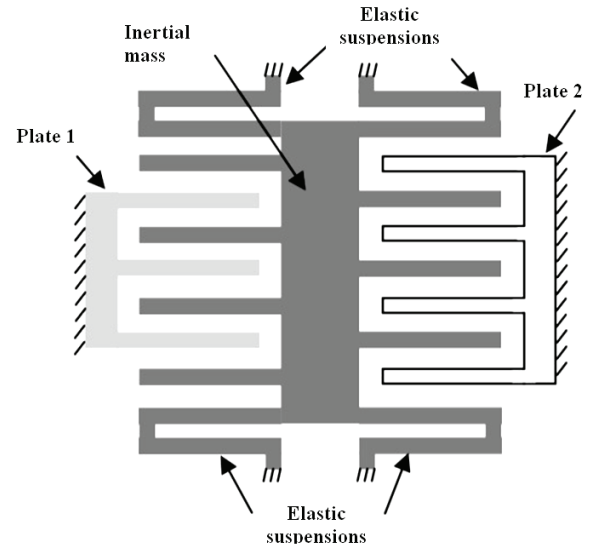


Fig. 1. Design of differential capacitive MEMS – gravimeter with oppositely-pin arrangement of the plates' electrodes [12]

Elastic suspensions can be straight and folded (Fig. 2).

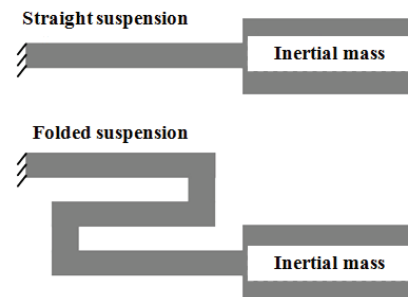


Fig. 2. Possible shape of elastic suspensions [12]

The choice of geometry of the elastic suspension is largely determined by the constraints of topology and technological processes. In order to obtain high sensitivity and small dimensions of suspension, it is necessary to reduce its width, but reducing the width leads to the fact that the suspension characteristics are significantly affected by the reproducibility of the technological process [13]. Increasing the width of the suspension, in order to reduce sensitivity to the deviations in the technological process, leads to the need for increasing its length, which increases the size of the crystal. As a compromise solution, a folded suspension can be used (folded beam, serpentine beam [12]).

For a more effective performance, the use of several capacitive transducers on one MEMS-plate is proposed [14, 15]. To ensure the dual-channel principle, symmetrically to one MEMS-plate, there is another MEMS-plate installed, completely identical to it, the signals of both are summed in the adder and transferred for further processing and amplification. The SE symmetry reduces dependence on

temperature and sensitivity along the axis and improves linearity. The impermeability of transducer is provided for by the anode connection of plates with each other. This makes packaging of elements easier and allows using gas attenuation in the sensing element.

Gravimeter is made with two channels, each of which contains one capacitive element in CG1 and CG2. They are identical and are fabricated in the form of two metallic movable and immovable plates separated by a dielectric, and two identical inertial masses m_1 and m_2 , attached to two moving plates CG1 and CG2 (Fig. 3). The outputs of capacitive elements CG1 and CG2 of both channels are connected to the input of the adder. The latter is connected to the input of the amplifier with additionally introduced protective ring whose output is connected through the digital module with the onboard computer (OC) input that computes the output signal of gravitational anomaly Δg . The connection of the adder, amplifier, digital module and OC in series is carried out using shielded coaxial cables to provide improved accuracy for measuring the anomalies in the acceleration of gravity.

The output electrical signals of capacitive elements of both channels enter the adder's input. The resulting useful analog signal will be proportional to the doubled signal of the acceleration of gravity and will enter the input of the amplifier with additionally introduced protective ring. Next, the amplified signal arrives at the input of the digital module where it will be converted into digital code and sent to the input of OC for subsequent calculation of gravitational anomaly Δg .

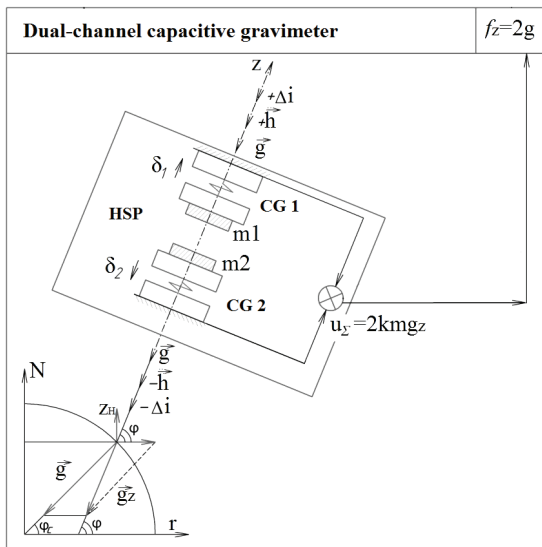


Fig. 3. Design of Dual-channel capacitive gravimeter

The calculation of coefficient of elasticity by using accurate analytical ratios is possible for simple forms of suspension. For the complex ones, approximate expressions are used. In particular, coefficient of elasticity of the folded suspension, shown in Fig. 4, in the first approximation can be calculated using the following formula [12]:

$$K = \frac{12EI}{(2N+3)l^3} = \frac{Etw^3}{(2N+3)l^3}, \tag{1}$$

where E is the modulus of elasticity of the suspension's material, I is the moment of inertia of the suspension cross section, t is the suspension thickness, w is the suspension width,

N is the number of folds on the suspension, l is the length of a segment of the folded suspension.

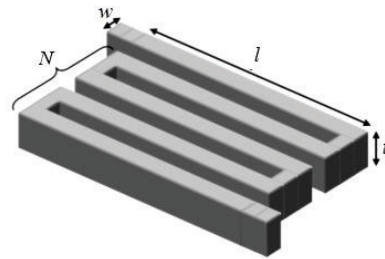


Fig. 4. Suspension of complex shape [12]

In order to obtain a more accurate value of coefficient of elasticity of the suspension with complex shape, in particular folded suspension, it is optimal to use finite-element modeling.

Thus, aviation gravimetric system provides a significant increase in the accuracy of measuring the anomalies in the acceleration of gravity. The AGS proposed has the following basic advantages over the known systems due to the use of DCG:

- through the use of two channels, such measurement errors are completely absent, which are caused by influence of the vertical acceleration and instrumental errors Δi ;
- other errors are partially eliminated due to the use of horizontal stabilized platform (HSP);
- when using frequency in 0.1 rad/s, residual errors will be filtered out.

Therefore, the accuracy of AGS with DCG exceeds all known analogues.

4. 2. Study of stability of the system with MEMS DCG

When carrying out measurements, there is always a transition process, at which a signal at the output of the measurement tool significantly changes over time. This is due to the inertial properties of measurement tool, which cause the occurrence of a dynamic error [16].

The examined system is nonlinear, similar to most systems in nature and technology.

In paper [17], characteristic equation of the DCG system was obtained:

$$D(p) = T^2 p^2 + 2 \cdot \xi \cdot T \cdot p + (1 + K_{DCG}) = 100p^2 + 14p + (1 + 40). \tag{2}$$

In a stable DCG system, at any real perturbation in it, adjustable magnitude in the transition process will not infinitely deviate from the set value. There are many criteria for stability, both analytical and graphic. The most common are the Nyquist criterion and the Hurwitz criterion. We shall estimate stability of the DCG system by these criteria.

The Hurwitz stability criterion: in order for the system of automated control to be stable, it is necessary and sufficient that all Hurwitz specifiers had signs identical to the sign of the senior factor of characteristic equation a_n , that is, positive at $a_{n-1} > 0$ [4].

Thus, the necessary and sufficient condition of stability for a system of the second order is positivity of factors of characteristic equation. In our system, we observe the following:

$$a_0 = T^2 = 100 > 0,$$

$$a_1 = 2 \cdot \xi \cdot T = 14 > 0, \quad (3)$$

$$a_2 = 1 + K = 40 > 0.$$

Thus, by the Hurwitz stability criterion, the DCG system is stable.

Transfer function of DCG by the AG channel for the output voltage [17]:

$$W_{DCG}(p) = \frac{K_{DCG}}{T_1 p^2 + T_2 p + 1}, \quad (4)$$

where K_{DCG} (static coefficient of DCG transfer; T_1 and T_2 (factors that determine time constants of the second order object.

In order to examine DCG on stability by the Nyquist criterion, we shall use transfer function of DCG:

$$W_{DCG}(p) = \frac{40}{100p^2 + 14p + 1}. \quad (5)$$

We substitute $p=j\omega$ into equality (5) and obtain the DCG transfer frequency function:

$$W(j\omega) = \frac{40}{-100\omega^2 + 14j\omega + 1} = \frac{40(1-100\omega^2 + 14j\omega)}{(1-100\omega^2)^2 + j(-14\omega)^2} = X(\omega) + jY(\omega), \quad (6)$$

where $X(\omega)$, $Y(\omega)$ are the real and imaginary parts of the DCG transfer frequency function, respectively.

Let us select from equality (6) the actual and imaginary part and find the intersection point of amplitude and phase characteristic (APC) of actual axis $X(\omega)$:

$$\begin{cases} X(\omega) = \frac{40(1-100\omega^2)}{(1-100\omega^2)^2 + j(-14\omega)^2}; \\ Y(\omega) = \frac{40 \cdot 14\omega}{(1-100\omega^2)^2 + j(-14\omega)^2}; \end{cases} \quad (7)$$

$$X(0) = 40.$$

Based on the calculated data, we plot APC (Fig. 5) in the MatLab programming environment (Nyquist hodograph).

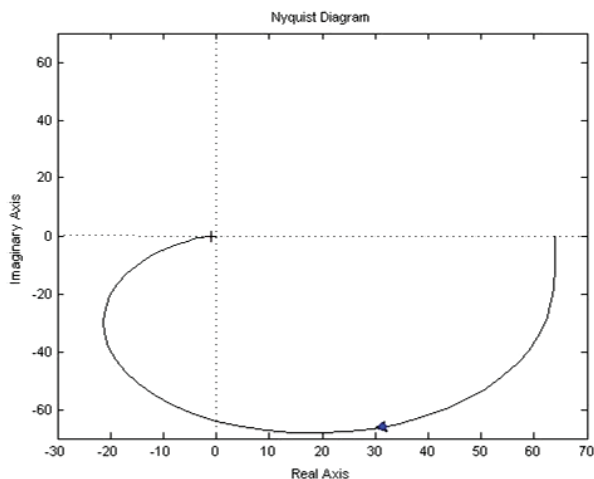


Fig. 5. Amplitude and phase characteristic of DCG

In order for the DCG system to be stable, it is necessary and sufficient that the Nyquist hodograph does not cover the point with coordinates $(-1; j0)$. As we can see from Fig. 5, the point is not covered; therefore, the DCG system is stable.

4. 3. Software development for the simulation of DCG performance under the action of external perturbations

If we divide equation of the DCG motion [17] by m , then we receive:

$$\ddot{x} + 2 \cdot \xi \omega_0 \dot{x} + \omega_0^2 x = -2g_z, \quad (8)$$

where ξ is the factor of dampening; ω_0 is the DCG own frequency.

Considering that the real design of any gravimeter (including DCG) will have residual instrumental errors due to temperature influences, pressure changes of the environment and other factors, as well as residual errors from the effects of vertical acceleration, which can lead to the nonlinearity of equation of the DCG motion in our case, we shall rewrite equations (8) in the form [4]:

$$m\ddot{x} + \dot{x}[2n - L\sin(\omega t + \varepsilon)] + \omega_0^2 x = N\sin \omega t, \quad (9)$$

where $L = mw_a$, $N = mw_b$ are the vibration parameters; w_a , w_b are the amplitudes of vibration accelerations.

Assume that

$$M(t) = 2n - L\sin(\omega t + \varepsilon),$$

and $D(t) = \omega_0^2$, then:

$$\ddot{x} + \dot{x}M(t) + D(t)x = 0, \quad (10)$$

where $M(t)$ and $D(t)$ are the T-periodic functions.

Equation of form (10) without changing the characteristics of indicators can be reduced to similar, where $M(t) = \text{const}$.

Let

$$\int_0^t M(t_1) dt_1 = \Psi t + M_1(t), \quad (11)$$

where $\Psi = 2n$;

$$M(t_1) = \int_0^t (M(t_1) - \Psi) dt = \frac{L}{\omega} \cos(\omega t + \varepsilon).$$

After all mathematical transformations, the equations can be written down in the form:

$$\ddot{x}' + 2\xi\omega_0 \dot{x}' + (\omega_0^2 + v_1 w_b \sin \omega t) x' = 0,005 w_a \sin \omega t, \quad (12)$$

where $v_1 = \frac{v_0}{w_b}$.

Thus, we obtained equation (12) of the Mathieu-Hill type with regard to residual errors from the influences of instrumental errors and \dot{h} , which is convenient for the simulation by PC [18].

Software for the simulation of DCG performance under the action of external perturbations was developed taking into account (12) in the C# programming environment. C# (pronounced C-sharp) is an object-oriented programming language, developed under the aegis of Microsoft Research (Microsoft Corp.) [19].

The program interface consists of the window (Fig. 6), in which parameters for simulation are assigned and its results are displayed in the form of tables and graphs. In the process of developing a program, equation (12) was transformed in the form:

$$\begin{aligned} \dot{x}' &= \dot{Y}; \\ \dot{Y} &= 0,005w_a \sin \omega t - \\ &- 2\xi\omega_0\dot{x}' - (\omega_0^2 + v_1w_b \sin \omega t)x'. \end{aligned} \tag{13}$$

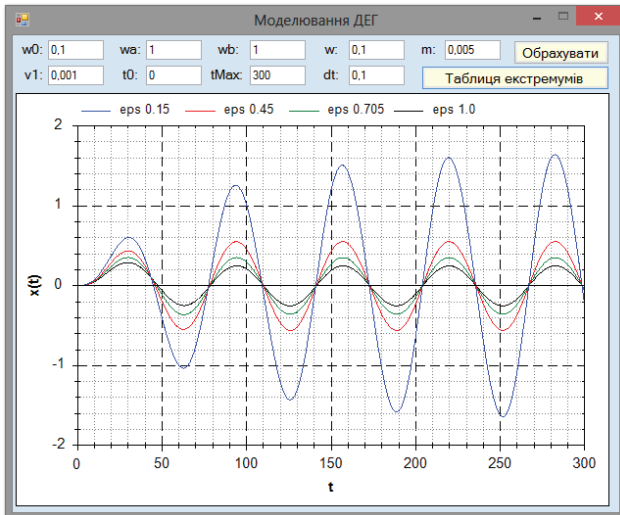


Fig. 6. PC program interface for the simulation of DCG performance under the action of external perturbations

Upon setting initial conditions and introducing machine variables ($z = \xi$, $w = \omega$, $wA = w_a$, $wB = w_b$, $T = t$), expression (13) can be written down in the form

$$\begin{aligned} \dot{X}' &= Y; \\ Y &= \sin(w*T)*(AA - \\ &- BB*X') - CC*Y - ww*X'. \end{aligned} \tag{14}$$

Using the Runge-Kutta methods of the fourth order for the integration of a system of differential equations, we receive solutions for system (15):

$$\begin{aligned} X'(T+H) &= \\ &= X'(T) + \frac{1}{6} * [X1 + X4 + 2. * (X2 + X3)]; \\ Y(T+H) &= Y(T) + \frac{1}{6} * [Y1 + Y2 + 2. * (Y2 + Y3)], \end{aligned} \tag{15}$$

where coefficients X1, X2, X3, X4, Y1, Y2, Y3, Y4 can be defined as follows:

$$\begin{aligned} X1 &= H * Y; Y1 = H * [\sin(w * T) * (AA - BB * x) - \\ &- CC * Y - ww * x]; X2 = H * (Y - 0,5 * Y1); \end{aligned}$$

$$Y2 = H * \left\{ \begin{aligned} &\sin[w * (T + 0,5 * H)] * [AA - BB * (X + 0,5 * X1)] - \\ &- CC * [Y + 0,5 * Y1] - ww * (X + 0,5 * X1) \end{aligned} \right\};$$

$$X3 = H * (Y + 0,5 * Y2);$$

$$Y3 = H * \left\{ \begin{aligned} &\sin[w * (T + 0,5 * H)] * [AA - BB * (X + 0,5 * X2)] - \\ &- CC * (Y + 0,5 * Y2) - ww * (X + 0,5 * X2) \end{aligned} \right\};$$

$$X4 = H * (Y + Y3);$$

$$Y4 = H * \left\{ \begin{aligned} &\sin[w * (T + H)] * [AA - BB * (X + X3)] - \\ &- CC * (Y + Y3) - ww * (X + X3) \end{aligned} \right\}.$$

In Table 1 we shall represent all parameters that appear in the calculations and the program interface.

Table 1

Name of symbols used in the program		
No. of entry	Symbol	Name
1	ξ (eps)	DCG damping coefficient
2	w	Frequency of oscillation
3	w0	DCG own frequency
4	w_a	Amplitude of perturbing influence along the Oz axis
5	w_b	Amplitude of perturbing influence along the Oy axis
6	t0	Starting time
7	tmax	Integration limit (end time)
8	dt	Integration step
9	m	DCG sensing element mass

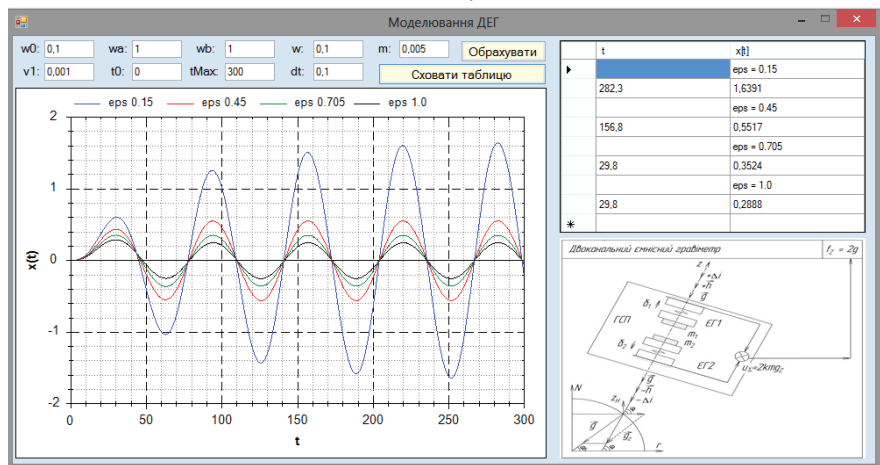


Fig. 7. Expanded PC program interface for the simulation of DCG performance under the action of external perturbations

After entering data into the appropriate fields of the program, for the calculation (or recalculation), it is necessary to click on the “Calculate” button – and the graphs will change. To receive numerical values of the extrema, it is necessary to click on the “Table of extrema” button. The program window will expand (Fig. 7) and there will appear the required table on the right side as well as a schematic representation of the DCG structure.

5. Results of the PC simulation of capacitive MEMS gravimeter

5.1. Simulation of the suspension of complex shape

In order to obtain a more accurate value of coefficient of elasticity of the suspension of complex shape, in particular

folded suspension, it is optimal to use finite-element modeling. In this work, suspension simulation was conducted using the SolidWork software. We created a finite-element model of the suspension that describes the elastic element. A breakdown was achieved by the Solid element intended for solving elastic deformations tasks. The suspension model and the finite element grid are shown in Fig. 8. In the area labeled by strokes, we set a limiting condition that prohibits any displacement (the fixed end), and at the other end of the suspension, the load was assigned.

Results of the calculation of deformation and suspension are shown in Fig. 9. The magnitude of the impact equaled $10 \mu\text{N}$, displacement of the end of the elastic element reached $0.5 \mu\text{m}$.

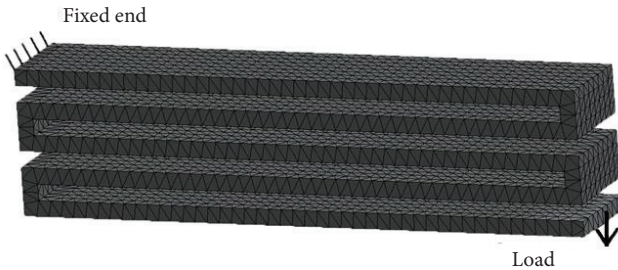


Fig. 8. Grid of finite elements of suspension with imposed conditions

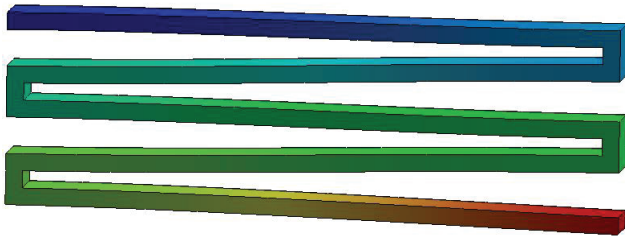


Fig. 9. Results of the simulation of folded suspension

5. 2. Results of the simulation of adverse resonances

1. Let us analyze the case that is the worst in terms of the occurrence of resonance, $\omega = \omega_0 = 0.1 \text{ rad/s}$. By the digital modeling of parametric equation (12) of DCG on PC, we received graphs of functional dependency $x=f(t)$ for the case when the base which supports the examined DCG is exposed to the action of perturbing influences, for which $w_a = w_b = 1 \text{ m/s}^2$ along the Oy and Oz axes, respectively. We set the value of relative attenuation coefficient ξ : 0.15; 0.45; 0.705; 1. It was experimentally determined that at low damping $\xi = 0.15$, the resonance is possible. In the case of increasing the damping, amplitude of the established oscillations is reduced (Fig. 10 and Table 2).

2. Let us analyze the DCG performance at $\omega = 2\omega_0 = 0.2 \text{ rad/s}$. We obtained dependences $x=f(t)$ for values $w_a = w_b = 1 \text{ m/s}^2$ and $\xi = 0.15; 0.45; 0.705; 1$, which indicate that as a result of increased damping, the DCG oscillations are aligned and tend to the ideal established oscillations. With increasing ξ , amplitude of the established forced DCG oscillations decreases. Resonance does not occur even at low damping, for example, at $\xi = 0.15$ (Table 2, Fig. 11).

As can be seen from the graphs in Fig. 11, the DCG oscillations enter the established mode in $t \leq 50 \text{ s}$, which is also quite satisfactory.

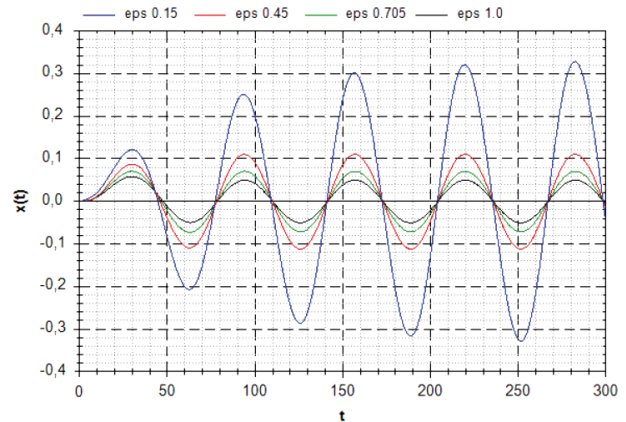


Fig. 10. Graph of change in the amplitude of initial signal at $\omega = \omega_0 = 0.1 \text{ rad/s}$ for $\xi = 1; 0.705; 0.45; 0.15$

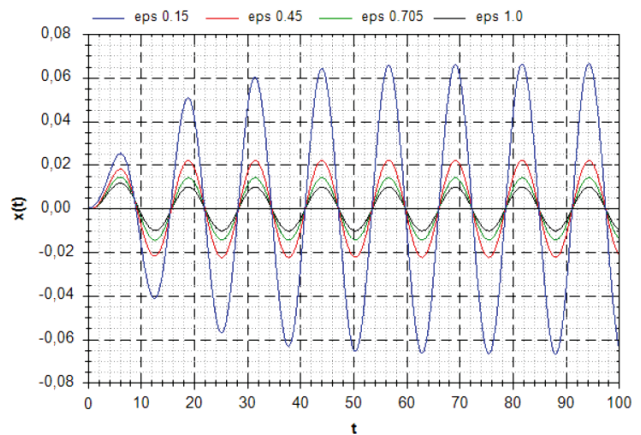


Fig. 11. Graph of change in the amplitude of initial signal $x=x'(t)$ at $\omega = 2\omega_0 = 0.2 \text{ rad/s}$ for $\xi = 1; 0.705; 0.45; 0.15$

3. Let us analyze results for the ratio of frequencies $\omega = \omega_0/2 = 0.05 \text{ rad/s}$. We received dependence $x=f(t)$ for $w_a = w_b = 1 \text{ m/s}^2$. Relative damping coefficient ξ composed: 0.15; 0.45; 0.705; 1. It was determined that even for very low damping $\xi = 0.15$, there occurs the DCG resonance. In the case of increasing ξ , the device quickly enters the mode of established forced oscillations; the reduction in the amplitude of oscillations of the initial signal of the device is observed (Table 2, Fig. 12).

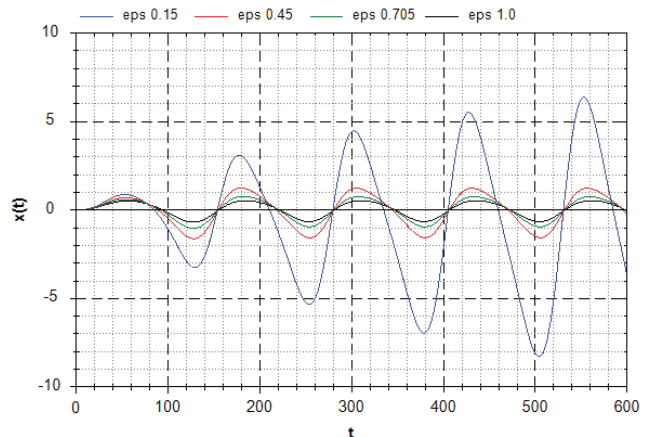


Fig. 12. Graph of change in the amplitude of initial signal $x=x'(t)$ at $2\omega = \omega_0 = 0.05 \text{ rad/s}$ for $\xi = 1; 0.705; 0.45; 0.15$

Table 2

Amplitudes of the forced DCG oscillations (simulation results)

w_0		$w=w_0=0,1$			
w_a		1	5	5	20
w_b		1	5	20	5
ξ	0,15	resonance			
	0,45	0,1103	0,5333	0,6421	2,1332
	0,705	0,0705	0,3398	0,31	1,3594
	1	0,0578	0,2578	0,2046	1,031
w_0		$w=w_0*2=0,2$			
w_a		1	5	5	20
w_b		1	5	20	5
ξ	0,15	0,0133	0,0666	0,0665	0,2665
	0,45	0,0044	0,0222	0,0221	0,0888
	0,705	0,0029	0,0145	0,0142	0,0579
	1	0,0024	0,0118	0,0116	0,0473
w_0		$2w=w_0=0,05$			
w_a		1	3	3	15
w_b		1	3	15	3
ξ	0,15	resonance			
	0,45	0,4304	1,2441	1,244	6,2201
	0,705	0,2744	0,7658	0,7656	3,8292
	1	0,2121	0,5326	0,5322	2,6628

6. Discussion of results of the simulation of performance and design of dual-channel capacitive gravimeter under the action of external perturbations

Based on the finite-element simulation data, we computed coefficient of elasticity of the suspension, equal to 16.7 N/m, which yields the total coefficient of elasticity, equal to 66.7 N/m for all four suspensions. As far as analytically calculated magnitude is concerned, then the error is 4 %. Coefficient of elasticity of the suspension allows us to calculate such important characteristics of a MEMS gravimeter as its own frequency, as well as absolute damping coefficient and relative damping factor [12].

Let us analyze dependences $x=f(t)$ for the three cases of the most unfavorable frequencies, similar to the previous paragraph, but at different values of amplitudes along the Oz and Oy axes:

1. Analysis of obtained dependences $x=f(t)$ for $\omega=\omega_0=0,1$ rad/s at different values of amplitudes of perturbing impact along the Oz and Oy axes.

In the first case, the amplitude perturbations along both axes are equal to $w_a=w_b=5$ m/s², ξ : 0.15; 0.45; 0.705; 1 revealed that in this case, the amplitude values of established forced DCG oscillations are five times larger than those in the previous case for respective ξ . Resonance is possible at low damping $\xi=0.15$, similar to the previous case (Table 2).

We defined dependences $x=f(t)$ when amplitude perturbations along the Oz axis $w_a=5$ m/s², and along the Oy axis are 4 times larger than those in the previous case $w_b=20$ m/s² ($\omega=\omega_0=0.1$ rad/s). Such amplitude values of the established forced oscillations are slightly different from the previous corresponding oscillations $x=f(t)$. This confirms the conclusion that is drawn as a result of analysis of static errors in DCG that its performance is not affected by horizontal ac-

celeration. The nature of the damping influence is the same as in the previous cases (Table 2).

We obtained dependences $x=f(t)$ when amplitude perturbation along the Oz axis is 4 times larger than in the second case, $w_a=20$ m/s², and along the Oy axis $w_b=5$ m/s², ξ : 0.15; 0.45; 0.705; 1, $\omega=\omega_0=0.1$ rad/s. Amplitude values of the established forced oscillations in this case are about five times larger than those in the second case (Table 2).

2. Analysis of obtained dependences $x=f(t)$ for $\omega=2\omega_0=0,2$ rad/s at different values of amplitudes of perturbing impact along the Oz and Oy axes.

We received dependences $x=f(t)$ when $w_a=w_b=5$ m/s², $\omega=2\omega_0=0.2$ rad/s for the same ξ . Even at low damping $\xi=0.15$, resonance is absent. In case of increasing ξ , the oscillations are aligned and approach the ideal established forced oscillations, the amplitudes of established forced oscillations are reduced, however, they are 5 times larger than the amplitudes that correspond to the previous case.

An analysis of dependences with parameters $w_a=5$ m/s², $w_b=20$ m/s², $\omega=2\omega_0=0.2$ rad/s (4 times larger than in the previous case) demonstrates that even at small damping $\xi=0.15$, resonance does not occur, however, similar to the previous cases, there are oscillations that, while increasing ξ , are aligned and tend to the established oscillations. The amplitude values of the DCG forced oscillations are insignificantly different from the corresponding values for the previous case (Table 2).

An analysis of dependence $x=f(t)$ for $w_a=20$ m/s² (4 times larger than in the second case), $w_b=5$ m/s², $\omega=2\omega_0=0.2$ rad/s, demonstrates that the amplitude values of the forced DSG oscillations are approximately three times larger than for the second at corresponding ξ . With increasing ξ , amplitude of the forced oscillations of the device decreases. Resonance does not occur even at low ξ , for example, $\xi=0.15$, however, there occur oscillations that are aligned and approach established values of the forced oscillations with increase in ξ , starting with $\xi=0.45$ (Table 2).

3. Analysis of obtained dependences $x=f(t)$ for $\omega=\omega_0/2=0,05$ rad/s at different values of amplitudes of perturbing impact along the Oz and Oy axes. Let us consider the case $w_a=w_b=3$ m/s² and the values of ξ similar to the previous variants. Here one can see (Table 2) that at low damping $\xi=0.15$, resonance occurs, but with increase in ξ , the device rapidly enters the mode of established forced oscillations. The amplitudes of the established forced oscillations decrease, however, they are 3 times larger than the amplitudes corresponding to the previous points.

Let us analyze dependences $x=f(t)$ at $w_a=3$ m/s², $w_b=15$ m/s² (5 times larger than those in the previous case). With increase in ξ , amplitudes of the forced oscillations of the DCG output decrease. Amplitude values of the forced oscillations of the devices are slightly different from the corresponding amplitude values for the previous case (Table 2).

We obtained dependences $x=f(t)$ for $w_a=15$ m/s², $w_b=3$ m/s² ($\omega=\omega_0/2=0.05$ rad/s). Amplitude values of the forced DCG oscillations in this case are about three times larger than those in the second case. With an increase in relative attenuation coefficient ξ , amplitude of the forced DCG oscillations decreases (Table 2).

Table 2 demonstrates that the increase in amplitudes of horizontal acceleration does not affect the amplitude of the forced DCG oscillations, and with an increase in damping value $\xi=0,705$, the main resonance and all distortions of the

signal disappear. Therefore, the new capacitive DCG might be used in the aviation gravimetry.

7. Conclusions

1. Using the Solid software package, we simulated the impact of load on a folded suspension. The magnitude of the impact equaled 10 μN , displacement of the end of the elastic element reached 0.5 μm . Based on these data, it is possible to refine the value of coefficient of elasticity of the folded suspension.

2. We received graphs of change in the initial signal for various values of frequency and amplitudes of perturbations. The graphs obtained demonstrate that:

– at frequency of perturbations $\omega=\omega_0=0.1$ rad/s, the main resonance occurs, the most dangerous for DCG;

– at frequencies $\omega=\omega_0/2=0.05$ rad/s, the initial signal is distorted;

– at frequencies $\omega=2\omega_0=0.2$ rad/s, the initial signal is not distorted;

– an increase in the amplitudes of horizontal acceleration does not affect the amplitude of the forced DCG oscillations.

Thus, when increasing damping value $\xi=0,705$, the main resonance and all distortions of the signal disappear.

Digital simulation of the influence of perturbations parameters on DCG, as well as its own parameters, confirmed an essential advantage of DCG over all known gravimeters – its high accuracy.

References

1. Bezvesil'na, O. M. Aviacijni gravimetrychni systemy ta gravimetry [Text] / O. M. Bezvesil'na. – Zhytomyr: ZhDTU, 2007. – 604 p.
2. Bykovskij, A. V. K voprosu o razrabotke malogabaritnogo ajerogravimetra [Text] / A. V. Bykovskij, A. V. Polynkov // Vestnik MGTU im. N. Je. Baumana. – 2013. – Issue 2 (14). – P. 32–41.
3. Girnjak, Ju. V. Mikroelektromehanichni systemy u suchasnomu pryladobuduvanni [Text] / Ju. V. Girnjak // Vymirjuval'na tehnika ta metrologija. – 2008. – Issue 69. – P. 97–102.
4. Korobijchuk, I. V. Tehnichni zasoby avtomatyzacii' [Text] / I. V. Korobijchuk. – Zhytomyr: ZhDTU, 2015. – 904 p.
5. Pat. № 113038. Aviacijna gravimetrychna systema dlja vymirjuvan' anomalij pryskorennja syly tjazhinnja. MPK: G01V 7/02, G01V 7/16, G01P 15/09 [Text] / Bezvesil'na O. M., Tkachuk A. G., Hyl'chenko T. V. – No. a201512205; declared: 09.12.2015; published: 25.11.2016, Byul. № 22.
6. Huang, Y. SGA-WZ: A New Strapdown Airborne Gravimeter [Text] / Y. Huang, A. V. Olesen, M. Wu, K. Zhang // Sensors. – 2012. – Vol. 12, Issue 12. – P. 9336–9348. doi: 10.3390/s120709336
7. Calvo, M. Time stability of spring and superconducting gravimeters through the analysis of very long gravity records [Text] / M. Calvo, J. Hinderer, S. Rosat, H. Legros, J.-P. Boy, B. Ducarme, W. Zurn // Journal of Geodynamics. – 2014. – Vol. 80. – P. 20–33. doi: 10.1016/j.jog.2014.04.009
8. Agostino, G. D. The new IMGC-02 transportable absolute gravimeter: measurement apparatus and applications in geophysics and volcanology [Text] / G. D. Agostino, S. Desogus, A. Germak, C. Origlia, D. Quagliotti, G. Berrino et. al. // Annals of geophysics. – 2008. – Vol. 51, Issue 1. – P. 39–49.
9. Roussel, C. Integration of a strapdown gravimeter system in an autonomous underwater vehicle [Text] / C. Roussel, J. Verdun, J. Cali, M. Maia, J. F. d'EU // ISPRS – International Archives of the Photogrammetry, Remote Sensing and Spatial Information Sciences. – 2015. – Vol. XL-5/W5. – P. 199–206. doi: 10.5194/isprsarchives-xl-5-w5-199-2015
10. Bykovskij, A. V. Ajerogravimetricheskij metod izmerenija gravitacionnyh anomalij [Text] / A. V. Bykovskij, A. V. Polynkov, V. D. Arsen'ev // Aviakosmicheskoe priborostroenie. – 2013. – Issue 12. – P. 11–19.
11. Pat. № 105122. Aviacijna gravimetrychna systema dlja vymirjuvannja anomalij pryskorennja syly tjazhinnja. MPK G01V 7/00 [Text] / Bezvesil'na O. M., Tkachuk A. G., Koz'ko K. S. – No. a201304061; declared: 01.04.2013; published: 10.04.2014, Byul. № 7.
12. Godovicyn, I. V. Raschet i modelirovanie osnovnyh parametrov differencial'nogo emkostnogo MJeMS-akselerometra [Text] / I. V. Godovicyn, D. A. Sajkin, R. A. Fedorov, V. V. Amelichev; A. L. Stempkovskiy (Ed.). – Moscow: IPPM RAN, 2010. – P. 642–647.
13. Shurygina, V. V. Dolgozhdannye MJeMS. Tehnologija malyh form [Text] / V. V. Shurygina // Jelektronika: Nauka, Tehnologija, Biznes. – 2002. – Issue 4. – P. 8–13.
14. Sovremennye MJeMS-giroskopy i akselerometry [Electronic resource]. – Available at: http://www.sovtest.ru/news/publications/sovremennye-mems_giroskopy-i-akselerometry/
15. Implications of Emerging Micro and Nanotechnology [Text]. – Washington, D.C., 2002. – 266 p. doi: 10.17226/10582
16. Afonin, A. A. O vozmozhnosti postroenija besplatformennogo upravljajushhego navigacionno-gravimetricheskogo kompleksa bespilotnogo letatel'nogo apparata [Text] / A. A. Afonin, A. S. Sulakov, G. G. Jamashev, D. A. Mihajlin, L. A. Mirzojan, D. V. Kurmakov // Trudy MAI. – 2013. – Issue 66. – P. 47–53.
17. Bezvesil'naja, E. N. Analiz metodicheskikh pogreshnostej dvuhkanal'nogo emkostnogo gravimetra [Text] / E. N. Bezvesil'naja, T. V. Hil'chenko // Sodruzhestvo. – 2016. – Issue 3 (3). – P. 51–54.
18. Dekker, K. Ustojchivost' metodov Runge-Kutty dlja zhestkih nelinejnyh differencial'nyh uravnenij [Text] / K. Dekker, Ja. Verwer. – Moscow: Mir, 1988. – 334 p.
19. Rukovodstvo po programmirovaniu na C# [Electronic resource]. – Microsoft. – Available at: <https://msdn.microsoft.com/en-us/library/67ef88bd.aspx>